NANO LETTERS

Letter

pubs.acs.org/NanoLett

Three-Dimensional Proton Beam Writing of Optically Active Coherent Vacancy Spins in Silicon Carbide

H. Kraus,*[,†,‡] D. Simin,[†] C. Kasper,[†] Y. Suda,[§] S. Kawabata,[§] W. Kada,[§] T. Honda,[‡,∥] Y. Hijikata,[∥] T. Ohshima,[‡] V. Dyakonov,[†,⊥] and G. V. Astakhov*[,†]

[†]Experimental Physics VI, Julius Maximilian University of Würzburg, 97074 Würzburg, Germany

[‡]National Institutes for Quantum and Radiological Science and Technology (QST), Takasaki, Gunma 370-1292, Japan

[§]Faculty of Science and Technology, Gunma University, Kiryu, Gunma 376-8515, Japan

[∥]Graduate School of Science and Engineering, Saitama University, Saitama 338-8570, Japan

[⊥]Bavarian Center for Applied Energy Research (ZAE Bayern), 97074 Würzburg, Germany

Supporting Information

ABSTRACT: Constructing quantum devices comprises various challenging tasks, especially when concerning their nanoscale geometry. For quantum color centers, the traditional approach is to fabricate the device structure after the nondeterministic placement of the centers. Reversing this approach, we present the controlled generation of quantum centers in silicon carbide (SiC) by focused proton beam in a noncomplex manner without need for pre- or postirradiation treatment. The generation depth and resolution can be predicted by matching the proton energy to the material's stopping power, and the amount of quantum centers at one specific sample volume is tunable from ensembles of millions to discernible single photon emitters. We identify the generated centers as silicon vacancies through their characteristic magnetic resonance signatures and demonstrate that they possess a long spin−echo coherence time of 42 ± 20 μs at room temperature. Our approach hence enables the fabrication of quantum hybrid nanodevices based on SiC platform, where spin centers are integrated into p-i-n diodes, photonic cavities, and mechanical resonators.

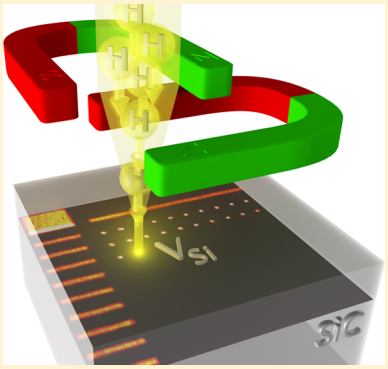

KEYWORDS: *Silicon carbide, atom-scale defects, proton beam writing, quantum coherence*

SiC is an excellent material system for optoelectronics and nanomechanics. For instance, unprecedented mass resolution has been shown using nanoelectromechanical (NEMS) devices based on SiC with fundamental frequencies above 100 MHz.[1] SiC-based photonic nanocavities with ultrabroadband operation from infrared to visible have been realized using heteroepitaxial growth of 3C-SiC on Si.[2] In addition to that, high-quality microdisk resonators[3] and nanobeam photonic crystals[4] have been fabricated using epitaxial, strain-free 4H-SiC layers. Compared to other wide-bandgap materials like GaN or diamond, SiC benefits from the low cost and CMOS-compatible technologies. Thus, 4H-SiC avalanche photodiodes (APD) are capable of detecting single UV photons at room temperature[5] and became commercially available recently.

Atom-scale color centers in SiC,[6] particularly silicon vacancies (V_{Si}), combine resonant optical addressability using near-infrared light,[7] spin memory above 20 ms without isotope purification,[8] and room-temperature functionality.[9,10] Because of their half-integer high-spin ground state,[10] the V_{Si} defects demonstrate high potential for quantum sensing applications,[11−13] like high-precision magnetometry[11,12,14−16] and thermometry.[11,17] It is highly desired to realize hybrid quantum systems based on SiC platform with obvious synergy, where defect spins are coupled to photonic/vibrational modes in a cavity or integrated into electronic circuits for on-chip manipulation.

Several research groups have already demonstrated spin-optoelectonic devices based on SiC. However, in these demonstrations, the vacancy related-defects were randomly generated in already fabricated nanostructures, like light-emitting diodes[18,19] or photonic structures.[20−22] The ability to deterministically induce the V_{Si} defect formation in a desired three-dimensional (3D) volume (at the nanoscale) and of desired density (down to single defects) is an important technological breakthrough not only because it enables spin-based quantum hybrid devices but also because it provides high degree of integration and scalability.

In this Letter, we demonstrate a simple, maskless method to perform 3D engineering of V_{Si} centers in SiC devices and nanostructures using proton beam writing (PBW). The depth at which the vacancies are generated is controlled by the proton energy, while the lateral resolution is obtained through proton beam focusing. No postirradiation treatment is required, and the number of defects within a selected volume can be varied

Received: December 29, 2016
Revised: March 22, 2017
Published: March 28, 2017

DOI: 10.1021/acs.nanolett.6b05395
Nano Lett. 2017, 17, 2865−2870

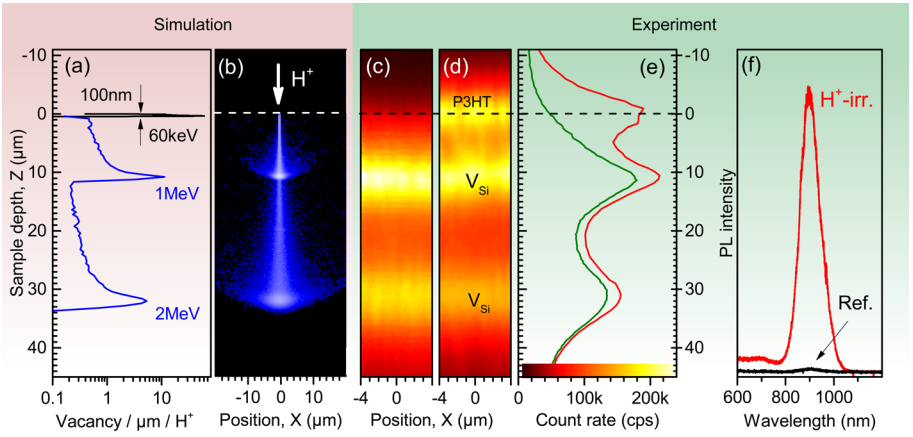

Figure 1. Proton writing of silicon vacancy layers at different depths of a SiC crystal. (a) Simulated profile (Bragg curve) for subsequent irradiation with multiple energies. (b) Spatially resolved equivalent of the simulations in (a) for a focused proton beam. (c) *XZ* depth scan of the emission with excitation λ_{exc} = 785 nm and detection λ_D > 830 nm. Only the V_{Si} implantation layers contribute to the PL signal. (d) To observe the position of the surface, a 1 μm thick layer of a photoluminescent organic compound (P3HT) was spin-coated on the sample. (e) Depth profiles of the emission from (c) (green) and (d) (red) obtained after integration along the *X*-direction. (f) PL from a H^+-irradiated area (λ_{exc} = 532 nm, no long-pass filter) and from a nonirradiated area of the same SiC layer. The PL spectrum corresponds to the V_{Si} emission at room temperature.

from millions to singles by tuning the irradiation fluence. The proton (H^+) irradiation (subsequently creating hydrogen impurities) has no discernible influence on the crystal's properties we would expect, for example, from known dopants like nitrogen or phosphorus. We thus observe a long room-temperature spin coherence time of 40 μs in the proton-generated V_{Si} centers, which is comparable to that in pristine wafers.[8]

Now we present the first step from bulk to layer defect engineering, that is, a reduction of the dimensionality by one. To this end, we borrow the idea of implanting nitrogen ions at a certain depth to create NV centers via subsequent annealing.[23] However, our method differs in that instead of implanting a third material that creates, together with a lattice defect, an active quantum center, we rather displace silicon lattice atoms by ion collisions. The passage of accelerated ions through a crystal, and their displacement energy deposition location, is governed by the quantum mechanical Bethe−Bloch equation for charged heavy particles.[24] Statistically, most ions deposit the bulk of their energy at a specific crystal depth, the Bragg peak. We exploit this property to displace silicon atoms at the Bragg peak position, directly creating an ion-energy tunable layer of silicon vacancies. Note that annealing (e.g., for activating an NV center at an implanted N site) is not necessary in this case, significantly reducing parameter space and complexity.[25,26] Indeed, annealing is expected to heal the desired V_{Si} already at moderate temperatures.[27] The displacement statistics, lateral ion straggle, and Bragg peak position can be calculated by means of a Monte Carlo simulation, for which we use the well-established SRIM software.[28] Comparing this calculation for different ions, we deduce that lighter ions, needing lower energies to reach the same implantation depth, are expected to have narrower Bragg peaks and damage the lattice less than heavier ions.

In our experiments, we use a high-purity semi-insulating (HPSI) 4H-SiC crystal, obtained from CREE, which is uniformly irradiated with subsequently E_{H^+} = 1 MeV and E_{H^+} = 2 MeV protons to an irradiation fluence of $\Phi = 1 \times 10^{13}$ cm^{-2} for each energy. A SRIM simulation for these energies predicts a defect distribution with Bragg peaks at depths of $\mathcal{Z}$(1 MeV) = 10.8 μm and $\mathcal{Z}$(2 MeV) = 31.9 μm, as shown in Figure 1a,b. In the 4H polytype, when considering the constituents' displacement energies,[29,30] one proton generates almost equal shares of silicon (V_{Si}) and carbon (V_C) vacancies. We calculate the average number of vacancies created per incoming proton (H^+) to $\mathcal{N}$(1 MeV) = [13.4V_{Si}; 12.2V_C]/H^+ and $\mathcal{N}$(2 MeV) = [18.0V_{Si}; 16.3V_C]/H^+. Below we will compare this number with experimental data.

In a confocal surface-lateral/depth (*XZ*) measurement of the specimen in question, two layers of luminescent species are observed [Figure 1c]. We attribute these layers to the Bragg peaks of the multiple proton irradiation, noting that we are obviously not sensitive to any surface defects[31] when exciting (785 nm) and detecting in the optical operation region of silicon vacancies (above 830 nm).[32] To ascertain the distance of the luminescent layers from the surface, the sample was coated with a 1 μm thin layer of the luminescent organic molecule poly-3-(hexylthiophene) (P3HT).[33] The sample surface can then be easily distinguished [Figure 1d], and the implantation layers' respective relative depths can directly be assigned to the aforementioned stopping power simulations $\mathcal{Z}(E_{H^+})$ of Figure 1a. Note that significant broadening of the Bragg peaks of Figure 1e in comparison to the simulation of Figure 1a is caused by the depth resolution of our confocal setup (details are presented in the Supporting Information).

A comparison of the photoluminescence (PL) of irradiated areas (excititation 532 nm) to pristine areas [Figure 1f] shows a strong increase of near-infrared emission, in contrast to almost negligible visible emission. This concludes that the optically active defects created by proton irradiation are the V1/V2-type silicon vacancies.[7,34] Below, we unambiguously prove the creation of V2 through spin resonance. Thus, we show that the creation of multiple, individual layers of ensemble V_{Si} quantum centers is made possible by proton irradiation, with control over the depth via tuning the irradiation energy.

In the next step, we add lateral control to the V_{Si} location. For this, we used a focused E_{H^+} = 1.7 MeV proton microbeam with a spot size of 1 μm and a position resolution of 15 nm. An ultrapure epitaxially grown SiC layer was then irradiated with multiple patterns (#1−3, details below and in the Supporting

DOI: 10.1021/acs.nanolett.6b05395
Nano Lett. 2017, 17, 2865−2870

Information). Technically, the irradiation is performed in the manner of the seminal review paper,[35] as also discussed in Methods. Figure 2a demonstrates that the aforementioned

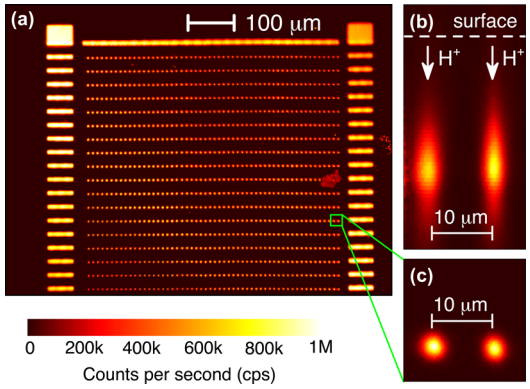

Figure 2. Three-dimensional PBW of silicon vacancies in insulating 4H-SiC. (a) *XY* confocal PL map of pattern #1, which is created using 1.7 MeV protons. The count rate is color-coded using logarithmic scale. (b) Zoom-in of a *XZ* confocal map along the depth direction. The vertical arrows represent schematically the focused proton (H^+) beams. (c) Zoom into the *XY* confocal PL map showing two irradiated sites with high resolution. The color scale codes the count rate in (b,c).

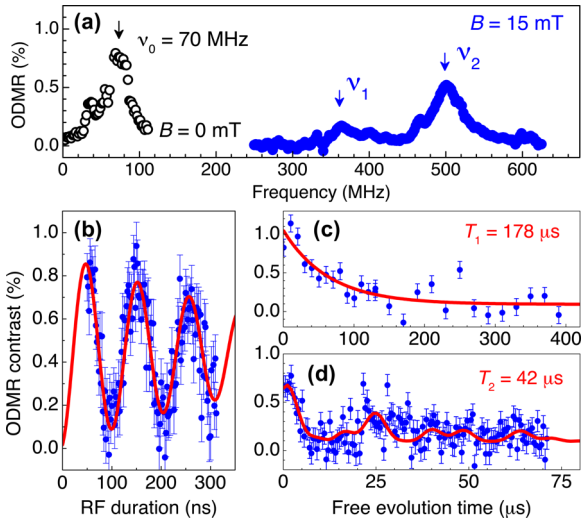

Figure 3. Room-temperature coherent control of 70 proton-written silicon vacancies. (a) ODMR spectra in zero magnetic field and in a magnetic field of 15 mT. (b) Rabi-oscillations obtained at the ν_1 spin resonance in B = 15 mT. (c) Measurement of the spin−lattice relaxation time T_1 = 178 ± 30 μs. The solid line is a monoexponential fit. (d) Spin−echo measurement of the spin coherence time T_2 = 42 ± 20 μs. The solid line is a fit with ESEEM.

PBW can be used to create a 2D array of luminescent sites. These sites are caused by the generation of the V_{Si} defects at a desired depth $\mathcal{Z}$ = 26 μm below the surface, as expected for 1.7 MeV protons [Figure 2b]. They are clearly separated and have circular form with $1/e^2$ diameter of about 2.5 μm [Figure 2c]. It is larger than the focused proton spot size on the surface because of proton straggling in the material, which is in accordance with the simulated distribution shown in Figure 1b.

To identify the generated color centers, we use optically detected magnetic resonance (ODMR). An example of the ODMR spectrum from a single site containing 70 emitters (irradiation pattern #2) is presented in Figure 3a. In zero magnetic field, we detect a single resonance at ν_0 = 70 MHz. Upon application of the magnetic field along the *c*-axis, the ODMR line is split and the corresponding resonances ν_1 and ν_2 are shifted toward higher frequencies. Their positions and relative amplitudes unambiguously point at the V2-type silicon vacancy.[12] We cannot exclude the formation of the V1-type silicon vacancies as well, however they show vanishingly small ODMR signal at room temperature.

Figure 3b−d demonstrates highly coherent properties of the generated V_{Si} spins, as required for the implementation of hybrid quantum devices. First, we observe Rabi oscillations [Figure 3b] using pulsed ODMR as described elsewhere.[8] Then, we measure the spin−lattice relaxation time T_1 = 178 ± 30 μs [Figure 3c]. Finally, using the Hahn echo pulse sequence we determine the spin coherence time T_2 = 42 ± 20 μs from the fit of the electron spin echo envelope modulation (ESEEM) in Figure 3d, which is known from the earlier reported bulk ensemble measurement.[8,36] The obtained T_1 and T_2 times are only marginally shorter than that in electron-irradiated samples.[8,36−38]

Having demonstrated 3D writing of V_{Si} spin ensembles, we decrease the irradiation fluence $\Phi < 10^{11}$ H^+/cm^2, which corresponds to less than 1000 protons per irradiation site (pattern #3). Under this condition, we now can distinguish single V_{Si} defects created in the proton track [Figure 4a]. The single photon emission is verified by the measurement of the second-order correlation function $g^{(2)}(0) < 0.5$ on one of these defects [Figure 4b] using fitting procedure as described elsewhere.[39] XY confocal scans at different Z presented in Supporting Information evidence that most of the single defects are localized within few microns at a certain depth. We verify that the count rate of a single V_{Si} emitter of ≈500 cps is much below the saturation level and it is then used to calibrate the number of defects at the proton irradiation sites.

Implantation reliability and reproducibility are crucial properties en route making ion irradiation one of the staples for defect introduction into quantum devices. To perform statistical analysis of the vacancy generation, the irradiation fluence is fixed for each line and increases line by line within each 2D array (see pattern description in Supporting Information). A statistic average over these lines is shown in Figure 4c−e with the measurement protocol explained in Supporting Information. For every irradiation site, we obtain the PL intensity from a Gaussian fit. In the Bragg peak region, the irradiation creates a lateral PL profile as shown in the inset of Figure 4c, which coincides well with the expected proton straggling from the Monte Carlo simulation of Figure 1b. Thus, we calculate an approximate number of created defects per incident proton by dividing the overall ensemble PL count rate through the PL count rate calibrated for a single V_{Si} emitter. Then, we have to consider that only a fraction of defects is detected within our confocal collection volume of 2.6 μm^3. According to our Monte Carlo simulations, this leads to the underestimating the whole amount of defects created by approximately 50%. The obtained number of V_{Si} per irradiation site in Figure 4c (symbols) takes all these aspects into account.

We found a normal distribution of the PL intensity over irradiation sites for high irradiation fluences $\Phi > 10^{11}$ H^+/cm^2 (or >1000 H^+ per site), as shown in Figure 4d. In case of low irradiation fluence, corresponding on average to 200 H^+ per site, the V_{Si} distribution is well described by the Poisson

DOI: 10.1021/acs.nanolett.6b05395
Nano Lett. 2017, 17, 2865−2870

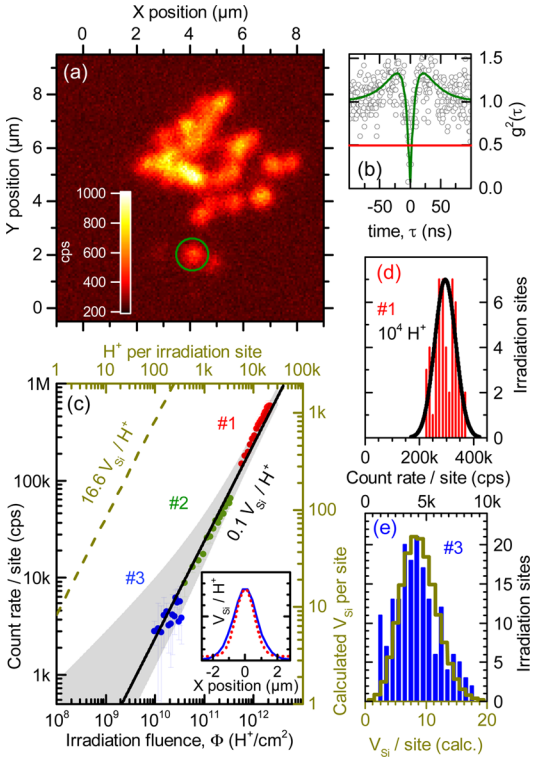

Figure 4. Statistical analysis of the silicon vacancy creation yield. (a) Close-up *XY* confocal scan of one implantation site ($\Phi = 1^{+4}_{-0.95} \times 10^9$ H^+/cm^2) at the Bragg peak depth. The circle shows a single V_{Si} center. (b) Intensity correlation measurement of the circled center in (a), with the second-order correlation function fit (solid line). (c) Brightness of the irradiation sites versus Φ for three different patterns. The solid line is a linear fit and the dashed line corresponds to the SRIM simulation. The confidence region for Φ is shown in gray. The inset depicts the simulated vacancy distribution at Bragg depth (solid line), coinciding with the measured averaged Gauss profiles of the implantation sites (dotted line). (d) Statistical distribution of the PL count rate per irradiation site for 10^4 protons. The solid line represents a normal distribution. (e) The same as (d) but for low proton number. The solid line represents a Poisson distribution of the number of the V_{Si} centers per irradiation site (lower axis) assuming 500 cps/V_{Si}.

statistics [Figure 4e] with a mean value of 9 V_{Si} within the microscope collection volume (or ≈20 V_{Si} per irradiation site).

As expected, this mean value scales linearly with the number of incident protons. Note that the relative accuracy of the proton irradiation fluence becomes worse for low Φ [gray region in Figure 4c]. The projection to the single V_{Si} intercept suggests the V_{Si} creation yield $\mathcal{N} \approx 0.1$ per proton [the solid line in Figure 4c]. At a first glance, this clashes with the theoretical prediction $\mathcal{N} = 16.6 V_{Si}/H^+$ [the dashed line in Figure 4c]. However, we need to consider that only a fraction of V_{Si} is photoactive. First, we specifically consider the negatively charged silicon vacancy, also called T_{V2a}.[40] The high-purity epitactically grown samples used here have only marginal doping, hence only a fraction of the created V_{Si} defects is negatively charged. Second, high-frequency electron nuclear double resonance experiments indicate[41] that the optically active negatively charged V_{Si} spin centers may be noncovalently bonded to the neutral carbon vacancy. The probability that a proton creates such a silicon−carbon vacancy configuration is indeed lower than that for an isolated vacancy. Another possibility to account for the low yield of photoactive defect is quenching of the silicon vacancy by the implanted hydrogen itself. Hydrogen atoms can connect to the carbon dangling bonds of a V_{Si}, passivating it, forming a hydrogen complex that does not show the desired photoactivity.[42] However, we expect this to be a minor effect, as at these acceleration energies, one hydrogen ion creates tens of vacancies, whereas one vacancy can accommodate up to four hydrogen atoms.

In terms of 3D defect engineering, the V_{Si} creation yield $\mathcal{N} < 1$ per single proton is an advantage, as it allows downscaling the nearly deterministic defect production to single defects.

We believe that 3D PBW of vacancy spins can be also performed at the nanoscale. Using low-energy protons, it should be possible to localize defect spins very close to the surface. Thus, the Monte Carlo simulations of Figure 1a for 60 keV give vertical confinement within 100 nm below the surface. We expect that focused proton irradiation through a pierced atomic force microscope tip can provide a lateral resolution down to 10 nm, similar to that demonstrated for nitrogen implantation into diamond.[43] Our approach hence paves a way for targeted positioning of single defect spins in SiC with nanometer precision in three dimensions. There is no need for pre- or postirradiation treatment, such as δ-doping during growth[44,45] and/or mask patterning[6,44,46] followed by subsequent annealing.[23,43−48] Optically addressable and highly coherent spin centers are generated in a simple, point-and-shoot fashion, which can be directly applied for the fabrication of hybride spin-electronic, spin-photonic, and spin-mechanic quantum nanodevices based on a technologically friendly SiC platform.

Methods. *Samples.* The experiments of Figure 1 were carried out on HPSI 4H-SiC and 6H-SiC wafers with resistivity above 10^5 Ohm·cm purchased by CREE. The experiments of Figures 2−4 were performed on an ultrapure epitaxially grown 4H-SiC also purchased from CREE. A 100 μm thick layer (residual nitrogen doping below 5.0×10^{14} cm^{-3}) was epitaxially grown on a 2-in. n-type 4H-SiC wafer. The substrate was then removed and the epitaxial layer was thinned down to 79 μm using chemical-mechanical polishing by NOVASiC. Prior optical measurements, the samples were immersed in a 5% hydrofluoric acid solution for 10 min to remove surface defects introduced during polishing. To render the sample surface visible, the semiconducting polymer P3HT was solved in chlorobenzene, and spin-coated onto the sample surface with 2500 rpm for 40 s. The layer thickness was measured with a Dektak profilometer to be of the order of 1 μm.

Proton Irradiation. The microbeam patterning was done at the TIARA irradiation facilities of QST Takasaki, Japan. The proton beam was generated by the single-ended particle accelerator with an energy range of 1−3 MeV, then focused to a typical beam size of 1×1 μm^2, which was estimated from a secondary electron image on a copper mesh obtained before each irradiation experiment.[49,50]

The irradiation targets were placed on an aluminum plate, and their positions were controlled by a 2-axis stage (Canon Precision, 40 mm travel at a precision of 20 nm) using a home-built software.[51] The irradiation beam current was observed by a beam dump (Faraday cup) connected to a picoamperemeter before and after irradiation. Additionally, the beam current through the sample holder was monitored during irradiation, to register fluctuations and deviations from the intended current and fluence.[52]

DOI: 10.1021/acs.nanolett.6b05395
Nano Lett. 2017, 17, 2865−2870

Confocal Microscopy. For both cw- and pulsed experiments, a 785 nm cw laser diode from Thorlabs (LD785-SE400) is used to excite the V_{Si} defects. To create laser pulses, an AOM from A&A Optoelectronic (MT250-A0 2−800) is placed in the laser path. The laser beam is fed into a single mode fiber and subsequently focused onto the defect spots with a 100× optical objective from Olympus with N.A. = 0.85 (LCPLN100XIR), optimized for the near-infrared spectrum. The laser power on the spot is approximately 500 μW. The PL is collected through the same objective, while the laser reflection is filtered out by an 830 nm and an 875 nm long-pass filters from Semrock and Edmund Optics. The PL is fed into a 10 μm glass fiber, which acts as a pinhole, and transferred to a single photon avalanche diode from Laser Components (COUNT-50N-FC). The signal is then processed further to the dual SPAD power supply also from Laser Components (DSN102) and finally registered by a time-to-digital converter from qutools (quTAU). The samples are mounted on a piezo stage from Thorlabs (NanoMax), allowing *XYZ* scans over 20 μm with 20 nm resolution. The piezo stage is then mounted on a motorized microscope translator with encoder from Thorlabs (MTME-FN1) with 50 mm traveling range and 0.3 μm repeatability. In all scans along the *Z*-direction, we use the SiC refractive index n_{SiC} = 2.6 to calculate the real depth.

The necessary cw-RF are provided by a signal generator from Stanford Research Systems (SG384). RF pulses are established by a switch from Mini-Circuits (ZASWA-2-50DR+). The signal is amplified by an 18 W amplifier from Vectawave (VBA1000-18) and applied to a 1 mm copper stripline on which the sample is placed. The circuit is terminated by a 50 Ohm resistor. Magnetic field dependent experiments are performed with a NdFeB magnet (grade N42) placed at a distinguished distance to the sample.

In order to perform Rabi, T_1 and T_2 measurements, a pulse sequence is programmed into the PulseBlasterESR-PRO 500 MHz card from SpinCore, which then supplies TTL pulses to the AOM and to the RF-switch accordingly. The necessary pulse sequences are described in detail in ref 8.

■ ASSOCIATED CONTENT

Supporting Information

The Supporting Information is available free of charge on the ACS Publications website at DOI: 10.1021/acs.nanolett.6b05395.

Detailed description of the proton irradiation pattern design and automated statistical analysis (PDF)

■ AUTHOR INFORMATION

Corresponding Authors

*E-mail: kraus@physik.uni-wuerzburg.de.

*E-mail: astakhov@physik.uni-wuerzburg.de.

ORCID

V. Dyakonov: 0000-0001-8725-9573

G. V. Astakhov: 0000-0003-1807-3534

Notes

The authors declare no competing financial interest.

■ ACKNOWLEDGMENTS

This work has been supported by the German Research Foundation (DFG) under Grants DY 18/13 and AS 310/5, by the ERA.Net RUS Plus program and the German Federal Ministry of Education and Research (BMBF) within project DIABASE, as well as by the JSPS KAKENHI JP16K13721 and JP26286047. H.K. acknowledges financing of specimens by the "Universitätsbund Würzburg" (No. 15-36), as well as the support of the German Academic Exchange Service (DAAD), with funds of the BMBF and EU Marie Curie Actions (DAAD P.R.I.M.E. 57183951).

■ REFERENCES

(1) Li, M.; Tang, H. X.; Roukes, M. L. *Nat. Nanotechnol.* **2007**, *2*, 114−120.

(2) Yamada, S.; Song, B.-S.; Asano, T.; Noda, S. *Appl. Phys. Lett.* **2011**, *99*, 201102.

(3) Magyar, A. P.; Bracher, D.; Lee, J. C.; Aharonovich, I.; Hu, E. L. *Appl. Phys. Lett.* **2014**, *104*, 051109.

(4) Bracher, D. O.; Hu, E. L. *Nano Lett.* **2015**, *15*, 6202−6207.

(5) Xin, X.; Yan, F.; Koeth, T. W.; Joseph, C.; Hu, J.; Wu, J.; Zhao, J. H. *Electron. Lett.* **2005**, *41*, 1192.

(6) Falk, A. L.; Buckley, B. B.; Calusine, G.; Koehl, W. F.; Dobrovitski, V. V.; Politi, A.; Zorman, C. A.; Feng, P. X. L.; Awschalom, D. D. *Nat. Commun.* **2013**, *4*, 1819.

(7) Riedel, D.; Fuchs, F.; Kraus, H.; Väth, S.; Sperlich, A.; Dyakonov, V.; Soltamova, A.; Baranov, P.; Ilyin, V.; Astakhov, G. V. *Phys. Rev. Lett.* **2012**, *109*, 226402.

(8) Simin, D.; Kraus, H.; Sperlich, A.; Ohshima, T.; Astakhov, G. V.; Dyakonov, V. *Phys. Rev. B: Condens. Matter Mater. Phys.* **2017**, *95*, 161201.

(9) Soltamov, V. A.; Soltamova, A. A.; Baranov, P. G.; Proskuryakov, I. I. *Phys. Rev. Lett.* **2012**, *108*, 226402.

(10) Kraus, H.; Soltamov, V. A.; Riedel, D.; Väth, S.; Fuchs, F.; Sperlich, A.; Baranov, P. G.; Dyakonov, V.; Astakhov, G. V. *Nat. Phys.* **2013**, *10*, 157−162.

(11) Kraus, H.; Soltamov, V. A.; Fuchs, F.; Simin, D.; Sperlich, A.; Baranov, P. G.; Astakhov, G. V.; Dyakonov, V. *Sci. Rep.* **2014**, *4*, 5303.

(12) Simin, D.; Soltamov, V. A.; Poshakinskiy, A. V.; Anisimov, A. N.; Babunts, R. A.; Tolmachev, D. O.; Mokhov, E. N.; Trupke, M.; Tarasenko, S. A.; Sperlich, A.; et al. *Phys. Rev. X* **2016**, *6*, 031014.

(13) Soykal, Ö. O.; Reinecke, T. L. *Phys. Rev. B: Condens. Matter Mater. Phys.* **2017**, *95*, 081405.

(14) Simin, D.; Fuchs, F.; Kraus, H.; Sperlich, A.; Baranov, P. G.; Astakhov, G. V.; Dyakonov, V. *Phys. Rev. Appl.* **2015**, *4*, 014009.

(15) Lee, S.-Y.; Niethammer, M.; Wrachtrup, J. *Phys. Rev. B: Condens. Matter Mater. Phys.* **2015**, *92*, 115201.

(16) Niethammer, M.; Widmann, M.; Lee, S.-Y.; Stenberg, P.; Kordina, O.; Ohshima, T.; Son, N. T.; Janzén, E.; Wrachtrup, J. *Phys. Rev. Appl.* **2016**, *6*, 034001.

(17) Anisimov, A. N.; Simin, D.; Soltamov, V. A.; Lebedev, S. P.; Baranov, P. G.; Astakhov, G. V.; Dyakonov, V. *Sci. Rep.* **2016**, *6*, 33301.

(18) Fuchs, F.; Soltamov, V. A.; Väth, S.; Baranov, P. G.; Mokhov, E. N.; Astakhov, G. V.; Dyakonov, V. *Sci. Rep.* **2013**, *3*, 1637.

(19) Lohrmann, A.; Iwamoto, N.; Bodrog, Z.; Castelletto, S.; Ohshima, T.; Karle, T. J.; Gali, A.; Prawer, S.; McCallum, J. C.; Johnson, B. C. *Nat. Commun.* **2015**, *6*, 7783.

(20) Calusine, G.; Politi, A.; Awschalom, D. D. *Phys. Rev. Appl.* **2016**, *6*, 014019.

(21) Bracher, D. O.; Zhang, X.; Hu, E. L. PNAS 2017, published online, DOI: 10.1073/pnas.1704219114.

(22) Radulaski, M.; Widmann, M.; Niethammer, M.; Zhang, J. L.; Lee, S.-Y.; Rendler, T.; Lagoudakis, K. G.; Son, N. T.; Janzén, E.; Ohshima, T. *Nano Lett.* **2017**, *17*, 1782−1786.

(23) Meijer, J.; Burchard, B.; Domhan, M.; Wittmann, C.; Gaebel, T.; Popa, I.; Jelezko, F.; Wrachtrup, J. *Appl. Phys. Lett.* **2005**, *87*, 261909.

(24) Ahmed, S. N. *Physics and Engineering of Radiation Detection*; Elsevier Science, 2014.

(25) Yamamoto, T.; Umeda, T.; Watanabe, K.; Onoda, S.; Markham, M. L.; Twitchen, D. J.; Naydenov, B.; McGuinness, L. P.; Teraji, T.; Koizumi, S.; et al. *Phys. Rev. B: Condens. Matter Mater. Phys.* **2013**, *88*, 075206.

DOI: 10.1021/acs.nanolett.6b05395
Nano Lett. 2017, 17, 2865−2870

(26) Naydenov, B.; Reinhard, F.; Lämmle, A.; Richter, V.; Kalish, R.; D'Haenens-Johansson, U. F. S.; Newton, M.; Jelezko, F.; Wrachtrup, J. *Appl. Phys. Lett.* **2010**, *97*, 242511.
(27) Castelletto, S.; Johnson, B. C.; Ivády, V.; Stavrias, N.; Umeda, T.; Gali, A.; Ohshima, T. *Nat. Mater.* **2013**, *13*, 151−156.
(28) Ziegler, J. F.; Ziegler, M. D.; Biersack, J. P. *Nucl. Instrum. Methods Phys. Res., Sect. B* **2010**, *268*, 1818−1823.
(29) Lefèvre, J.; Costantini, J. M.; Esnouf, S. *J. Appl. Phys.* **2009**, *105*, 023520.
(30) Steeds, J. W.; Evans, G. A.; Danks, L. R.; Furkert, S.; Voegeli, W.; Ismail, M. M.; Carosella, F. *Diamond Relat. Mater.* **2002**, *11*, 1923−1945.
(31) Lohrmann, A.; Castelletto, S.; Klein, J. R.; Ohshima, T.; Bosi, M.; Negri, M.; Lau, D. W. M.; Gibson, B. C.; Prawer, S.; McCallum, J. C.; et al. *Appl. Phys. Lett.* **2016**, *108*, 021107.
(32) Hain, T. C.; Fuchs, F.; Soltamov, V. A.; Baranov, P. G.; Astakhov, G. V.; Hertel, T.; Dyakonov, V. *J. Appl. Phys.* **2014**, *115*, 133508.
(33) Liedtke, M.; Sperlich, A.; Kraus, H.; Baumann, A.; Deibel, C.; Wirix, M. J. M.; Loos, J.; Cardona, C. M.; Dyakonov, V. *J. Am. Chem. Soc.* **2011**, *133*, 9088−9094.
(34) Sörman, E.; Son, N.; Chen, W.; Kordina, O.; Hallin, C.; Janzén, E. *Phys. Rev. B: Condens. Matter Mater. Phys.* **2000**, *61*, 2613−2620.
(35) Watt, F.; Breese, M. B. H.; Bettiol, A. A.; van Kan, J. A. *Mater. Today* **2007**, *10*, 20−29.
(36) Carter, S. G.; Soykal, Ö. O.; Dev, P.; Economou, S. E.; Glaser, E. R. *Phys. Rev. B: Condens. Matter Mater. Phys.* **2015**, *92*, 161202.
(37) Christle, D. J.; Falk, A. L.; Andrich, P.; Klimov, P. V.; Hassan, J. u.; Son, N. T.; Janzén, E.; Ohshima, T.; Awschalom, D. D. *Nat. Mater.* **2014**, *14*, 160−163.
(38) Widmann, M.; Lee, S.-Y.; Rendler, T.; Son, N. T.; Fedder, H.; Paik, S.; Yang, L.-P.; Zhao, N.; Yang, S.; Booker, I.; et al. *Nat. Mater.* **2014**, *14*, 164−168.
(39) Fuchs, F.; Stender, B.; Trupke, M.; Simin, D.; Pflaum, J.; Dyakonov, V.; Astakhov, G. V. *Nat. Commun.* **2015**, *6*, 7578.
(40) Mizuochi, N.; Yamasaki, S.; Takizawa, H.; Morishita, N.; Ohshima, T.; Itoh, H.; Isoya, J. *Phys. Rev. B: Condens. Matter Mater. Phys.* **2002**, *66*, 235202.
(41) Soltamov, V. A.; Yavkin, B. V.; Tolmachev, D. O.; Babunts, R. A.; Badalyan, A. G.; Davydov, V. Y.; Mokhov, E. N.; Proskuryakov, I. I.; Orlinskii, S. B.; Baranov, P. G. *Phys. Rev. Lett.* **2015**, *115*, 247602.
(42) Deak, P.; Gali, A.; Aradi, B. In *Silicon carbide: recent major advances*; Choyke, W. J., Matsunami, H., Pensl, G., Eds.; Springer, 2013.
(43) Pezzagna, S.; Wildanger, D.; Mazarov, P.; Wieck, A. D.; Sarov, Y.; Rangelow, I.; Naydenov, B.; Jelezko, F.; Hell, S. W.; Meijer, J. *Small* **2010**, *6*, 2117−2121.
(44) Ohno, K.; Joseph Heremans, F.; de las Casas, C. F.; Myers, B. A.; Alemán, B. J.; Bleszynski Jayich, A. C.; Awschalom, D. D. *Appl. Phys. Lett.* **2014**, *105*, 052406.
(45) McLellan, C. A.; Myers, B. A.; Kraemer, S.; Ohno, K.; Awschalom, D. D.; Bleszynski Jayich, A. C. *Nano Lett.* **2016**, *16*, 2450−2454.
(46) Toyli, D. M.; Weis, C. D.; Fuchs, G. D.; Schenkel, T.; Awschalom, D. D. *Nano Lett.* **2010**, *10*, 3168−3172.
(47) Lesik, M.; Spinicelli, P.; Pezzagna, S.; Happel, P.; Jacques, V.; Salord, O.; Rasser, B.; Delobbe, A.; Sudraud, P.; Tallaire, A.; et al. *Phys. Status Solidi A* **2013**, *210*, 2055−2059.
(48) Huang, Z.; Li, W. D.; Santori, C.; Acosta, V. M.; Faraon, A.; Ishikawa, T.; Wu, W.; Winston, D.; Williams, R. S.; Beausoleil, R. G. *Appl. Phys. Lett.* **2013**, *103*, 081906.
(49) Kamiya, T.; Suda, T.; Tanaka, R. *Nucl. Instrum. Methods Phys. Res., Sect. B* **1995**, *104*, 43−48.
(50) Kamiya, T.; Takano, K.; Ishii, Y.; Satoh, T.; Oikawa, M.; Ohkubo, T.; Haga, J.; Nishikawa, H.; Furuta, Y.; Uchiya, N.; et al. *Nucl. Instrum. Methods Phys. Res., Sect. B* **2009**, *267*, 2317−2320.
(51) Sakai, T.; Yasuda, R.; Iikura, H.; Nojima, T.; Matsubayashi, M.; Kada, W.; Kohka, M.; Satoh, T.; Ohkubo, T.; Ishii, Y.; et al. *Nucl. Instrum. Methods Phys. Res., Sect. B* **2013**, *306*, 299−301.
(52) Kada, W.; Yokoyama, A.; Koka, M.; Takano, K.; Satoh, T.; Kamiya, T. *Jpn. J. Appl. Phys.* **2012**, *51*, 06FB07.

DOI: 10.1021/acs.nanolett.6b05395
Nano Lett. 2017, 17, 2865−2870